Chapter 7

Study of Formation and Decay of Rare-Gas Excimers by Laser-Induced Fluorescence

Frédéric Marchal, Neermalsing Sewraj, Jean-Pierre Gardou, Nofel Merbahi and Mohammed Yousfi

Additional information is available at the end of the chapter

http://dx.doi.org/10.5772/intechopen.71942

Abstract

The aim of this chapter is to review the experimental and numerical techniques for the estimation of the laser-induced fluorescence (LIF) decay in rare gases using time-correlated single-photon counting. The advantages of single-photon counting technique are discussed by means of measurement uncertainty analysis. In addition, this chapter provides information concerning the application of this technique to filamentary dielectric barrier discharges (DBD) and radiation trapping of the resonant transitions.

Keywords: single-photon counting, VUV emission of rare gases, excimer formation and decay, laser-induced fluorescence, dielectric barrier discharges, radiation trapping

1. Introduction

Vacuum ultraviolet (VUV) radiation sources are of great interest for many applications such as photochemistry, surface treatment, sterilization, water treatment, photolithography and mercury-free lamps [1–4]. These applications often use dielectric barrier excimer lamps [5–11]. Optimization of these VUV sources requires numerical modeling associated with experimental characterization. The determination of the main mechanisms that lead to excimer formation or decay requires accurately determining the reaction rates.

The emission mechanisms of VUV radiations by rare gases are now reasonably understood [12–15]. Excimers correlated to the first metastable or resonant states are responsible for these emissions. Kinetic models of formation and decay of rare-gas excited states were developed and validated by laser-induced fluorescence (LIF) in the case of argon, krypton, xenon and krypton-xenon mixtures.

Indeed, kinetic studies of rare gases via VUV fluorescence decays, following a brief and selective multiphotonic excitation, recorded by using single-photon counting fluorescence are highly suitable for the determination of reliable kinetic models. Absorption and emission spectroscopies help to complete such studies based on time dependence of VUV fluorescence [12–16, 19].

In these experimental studies, VUV fluorescence was monitored by a VUV photomultiplier tube operating in the single-photon counting mode. The emission wavelength was selected by either a VUV monochromator for the recording of the emission spectra or a suitable VUV range passband interferential filter for the excitation spectra and fluorescence decay studies. A multichannel scaler operating with 16,384 channels and a time resolution of 5 ns were used to record the time variation of the VUV luminescence.

Due to the rather weak detected luminous flux, the histograms recorded are characterized by a large number of channels and a low counting rate per bin. The modeling of the fluorescence decay of excited species introduces a temporal function, representing the rate equation model of collisional and radiative decay in a pure gas or a gas mixture. As far as the number densities of excited species in the interaction volume remain low and the laser energy kept low enough to avoid multiphotonic ionization, this function can be fitted by a sum of exponential decays, each one characterized by its own decay frequency associated to a particular single excited state. The number of decay frequencies corresponds to the number of states involved in the formation-decay processes.

In order to determine the temporal evolution law, the experimental histograms must be processed by using the maximum likelihood method, applied to a Poisson distribution which is more suitable than the least squares method for histograms with a low counting rate per channel.

The aim of this chapter is to review the experimental and numerical techniques combined with spectroscopic studies for the estimation of the laser-induced fluorescence (LIF) decay in rare gases. The advantages of single-photon counting techniques are discussed by means of measurement uncertainty analysis. In addition, this chapter provides information concerning the application of these techniques to filamentary dielectric barrier discharges (DBD) and radiation trapping of the resonant transitions.

2. Mechanisms of VUV emissions by rare gases

2.1. Rare-gas excimers

The emission mechanisms of VUV radiation by rare gases are now reasonably understood. Excimers correlated to the first metastable or resonant states are responsible for these emissions. **Figure 1** gives an example of excited molecular states involved in VUV emission of the continua of krypton [17]. The first metastable state and the first resonant one are the precursors to the excimer states. Three-body collisional processes lead to the formation of the high vibrational levels of these excimers. In low-pressure conditions, the transition of these high vibrational levels correlated to the lowest atomic excited states toward the weakly bound ground-state dimers leads to the emission of the first continuum. The second continuum is observed at high pressures,

http://dx.doi.org/10.5772/intechopen.71942

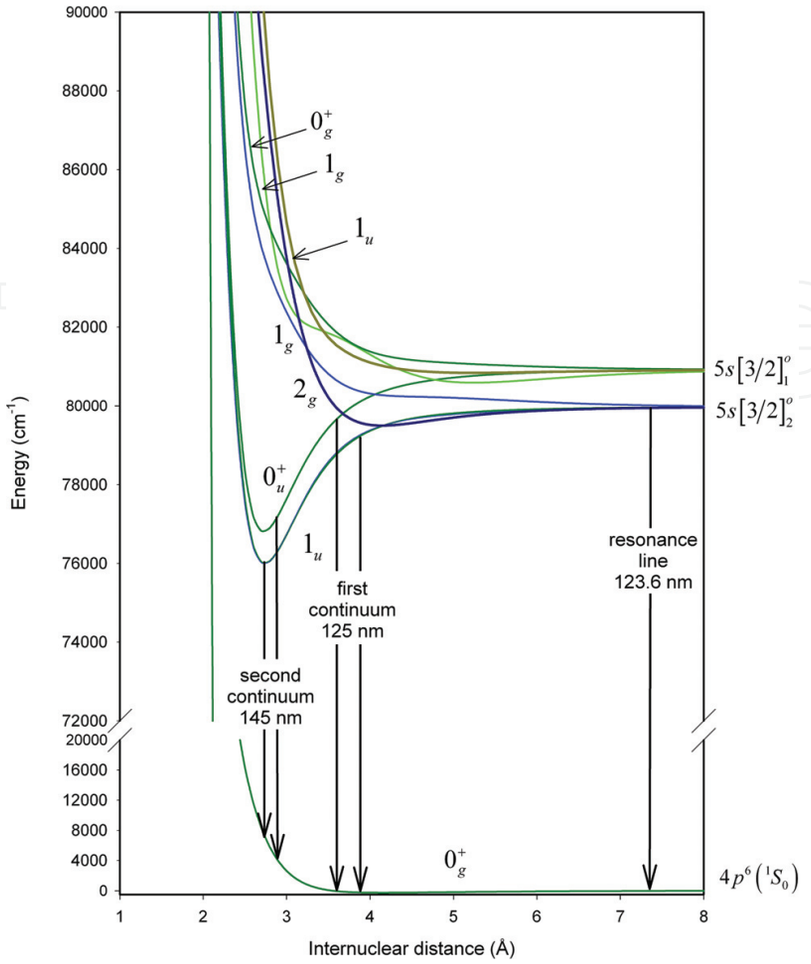

Figure 1. VUV emissions of the first and second continuum of krypton.

for which collisional relaxation of the high vibrational levels of these excimers is most likely. Thus, the second continuum, arising from radiative transitions of the lowest vibrational levels of the molecular excited states toward the ground state, dominates the spectrum.

2.2. Kinetic studies of VUV emissions of rare gases

Kinetic studies using laser-induced fluorescence (LIF) are highly suitable for the determination of kinetic models of formation and decay of rare-gas excimers.

The short-pulsed laser excitation populates only one atomic or molecular state (e.g. only the first resonant or only the first metastable states or the dissociative molecular states correlated to these atomic states). The initial time conditions are known at the beginning of the fluorescence decay, and the analysis of the time-correlated VUV fluorescence is greatly simplified. Non-selective excitation techniques such as electron beam, pulsed discharge or α-particles are not rigorous enough for the determination of kinetic models of the formation and decay of excimers because several processes compete (ionization, electron-ion recombination, electron-ion formation and destruction, second electron kinetics, etc.) [18, 21].

To illustrate the principle of kinetic studies of rare gases, we consider a simple atomic or molecular system of four states displayed in **Figure 2**. Just after the laser pulse, there is only

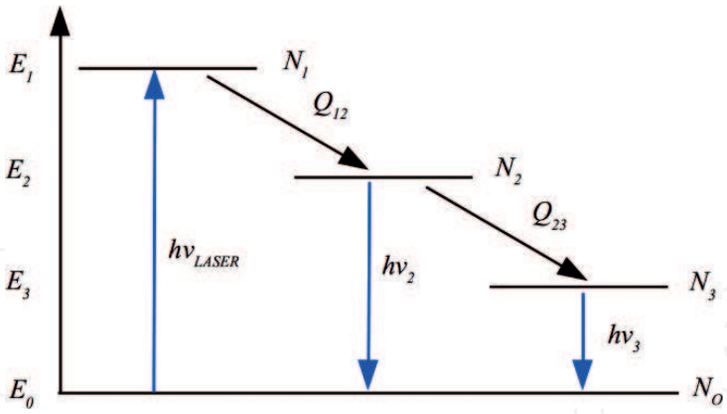

Figure 2. Simple model of laser-induced fluorescence for rare gases following the selective excitation of the first metastable state.

one exited state, for example, a metastable state noted N_1. The collisional decay of this state characterized by the quenching coefficient Q_{12} leads to populate a radiative state N_2. This state can also populate through a collisional reaction (characterized by the quenching coefficient Q_{23}), a lower level named N_3. This state can only decay by fluorescence emission. N_0 is the ground state.

This simple model can be used in the case of rare gases. The fluorescence coming from the N_2 molecular state is the first continuum, and the emission of the N_3 molecular state is called the second continuum. The exited state N_1 is the first metastable state.

The radiative decay frequencies α_1 and α_2 are relative to the two radiative states N_2 and N_3.

The number densities of the different states obey to the following ordinary differential equations:

$$\begin{cases} \dfrac{dN_1(t)}{dt} = -Q_{12}N_1(t) \\ \dfrac{dN_2(t)}{dt} = Q_{12}N_1(t) - (\alpha_1 + Q_{23})N_2(t) \\ \dfrac{dN_3(t)}{dt} = Q_{23}N_2(t) - \alpha_3 N_3(t) \end{cases} \tag{1}$$

provided that the laser pulse duration is short and the number densities of excited states can be comparatively negligible with respect to the number density of the ground state.

Thus, the initial conditions are

$$\begin{cases} N_1(t=0) = N_{10} \\ N_2(t=0) = 0 \\ N_3(t=0) = 0 \end{cases} \tag{2}$$

The number density N_0 of the ground state is supposed to remain constant. By solving the differential equations and considering the initial conditions, the time evolution of the number densities of the excited states are obtained:

$$\begin{cases} N_1(t) = N_{10}e^{-Q_1 t} \\ N_2(t) = N_{10}\dfrac{Q_{12}}{-Q_{12}+\alpha_1+Q_{23}}\left[e^{-Q_1 t} - e^{-(\alpha_2+Q_{23})t}\right] \\ N_3(t) = N_{10}Q_{12}Q_{23}\left[\dfrac{e^{-Q_1 t}}{(-Q_{12}+\alpha_1+Q_{23})(\alpha_3-Q_{12})} + \dfrac{e^{-(\alpha_2+Q_{23})t}}{(-Q_{12}+\alpha_1+Q_{23})^2} + \dfrac{e^{-\alpha_3 t}}{(-Q_{12}+\alpha_1+Q_{23})(-\alpha_3+Q_{12})}\right] \end{cases} \tag{3}$$

According to these expressions, the time decay of the VUV fluorescence intensities is given by

$$\begin{cases} I_{VUV2}(t') = \dfrac{\Omega}{4\pi}V_0 T\eta h\nu_2 \displaystyle\int_{t'}^{t'+\Delta t} \alpha_2 N_2(t)dt \\ I_{VUV3}(t') = \dfrac{\Omega}{4\pi}V_0 T\eta h\nu_3 \displaystyle\int_{t'}^{t'+\Delta t} \alpha_3 N_3(t)dt \end{cases} \tag{4}$$

where V_0 represents the observed volume, Ω is the solid angle of detection, T is the transmission of the optical system of detection, η is the efficiency of the photomultiplier at the fluorescence wavelength $\lambda_{VUV} = \frac{c}{\nu}$ and Δt is the time resolution of the detection system. The time acquisition of the fluorescence decay is supposed to be greater than the laser pulse width τ_L.

Overall, if the number densities of excited species in the interaction volume V_0 remains weak and the laser energy is low enough to avoid multiphotonic ionization, then collisions between excited species, ion recombination or electron collisions can be neglected. Thus, the simple model developed above can be generalized. The function *f*(t), which is the rate equation model of collisional and radiative decay in a neutral rare gas, is given by

$$f(t) = \sum_{p=1}^{p=D} a_p e^{-b_p t} + a_0 \tag{5}$$

where D is the number of excited states involved in the formation-decay processes, b_p is the decay frequency of each state and a_0 is the background noise of the detection system.

In pure rare gases, the decay frequency of the p^{th} term with respect to the pressure p is

$$b_p = \alpha_p + Q_p = \alpha_p + k_{2p}N_{0+}k_{3p}N_0^2 \tag{6}$$

where α_p represents the radiative decay frequency, k_{2p} is the two-body collisional rate constant and k_{3p} is the three-body collisional rate constant. The sum $k_{2p}N_{0+}k_{3p}N_0^2$ is the quenching coefficient Q_p. In rare-gas mixtures, the expression of the quenching coefficient is more complex due to the three-body heteronuclear collisional rate constant.

Modeling the experimental decay of the fluorescent intensities at various pressures is the best way to determine the rate equation model of collisional and radiative decay in rare gases. So, a numerical method of computing the decay frequencies b_p from the experimental data fitted with a sum of exponential terms is required. The rate constants, α_p, k_{2p} and k_{3p}, can be determined by processing all the experimental data of the decay frequencies measured in the

range of rare-gas pressures. Subsequently, kinetic schemes of formation and decay of rare-gas excimers can be proposed.

3. Single-photon counting method applied to the fluorescence decay recordings

3.1. Single-photon counting

As mentioned above, the time function of the fluorescence decay *f*(t) can be fitted by a sum of exponential terms if the number densities of excited space is very low compared to the number density of the ground state and if the laser excitation is short and selective enough. In order to fulfill these conditions, the laser intensity was considerably reduced to obtain a very low number density of the initially excited species. Thus, the intensity of the fluorescence becomes very weak, and the fluorescence photons are detected as separated pulses using a photomultiplier tube. In our experiments, only a few photoelectrons are detected per laser pulse. The average time intervals between signal pulses are wider than the time resolution of the detection system. In this case, the single-photon counting method using a photomultiplier is very effective and is superior to analog signal measurement in terms of stability and signal-to-noise ratio [22].

The single-photon counting method allows the number of photoelectrons detected to be in direct proportion of the fluorescence intensity. The signal pulses are counted by a multichannel scaler during the interval of two successive laser pulses, and the signal measured at each laser pulse period is accumulated at the laser pulse frequency to reproduce the fluorescence waveforms.

3.2. Photon counter system

The photon counter system is displayed in **Figure 3**. The fluorescence photons are collected by a photomultiplier tube (PMT). A non-inverting linear amplifier amplifies the negative output pulses of the PMT. The lower pulses are eliminated by the constant fraction discriminator, while the rest are reshaped. The output logic pulse corresponds to the point on the leading edge of the input pulse where the input pulse has risen to a fraction of its maximum amplitude. Thus, the time jitter is reduced, and the time resolution of the circuit system remains the same over a wide dynamic range of pulse amplitudes. The multichannel scaler counts events as a function of time. The laser trigger starts the counter, which segments photon count data into sequential time bins. The width of the bins can be set from a few nanoseconds to several milliseconds. The instrument records the number of photons that arrive in each bin. The multichannel scaler can be programmed to accumulate several records or set to free run. Each record is added to the current accumulator totals.

An example of time-resolved single-photon counting measurement of laser-induced florescence is shown in **Figure 4**. The experimental florescence is represented by a histogram with the bin number (proportional to the time) on x-axis and the counts on y-axis.

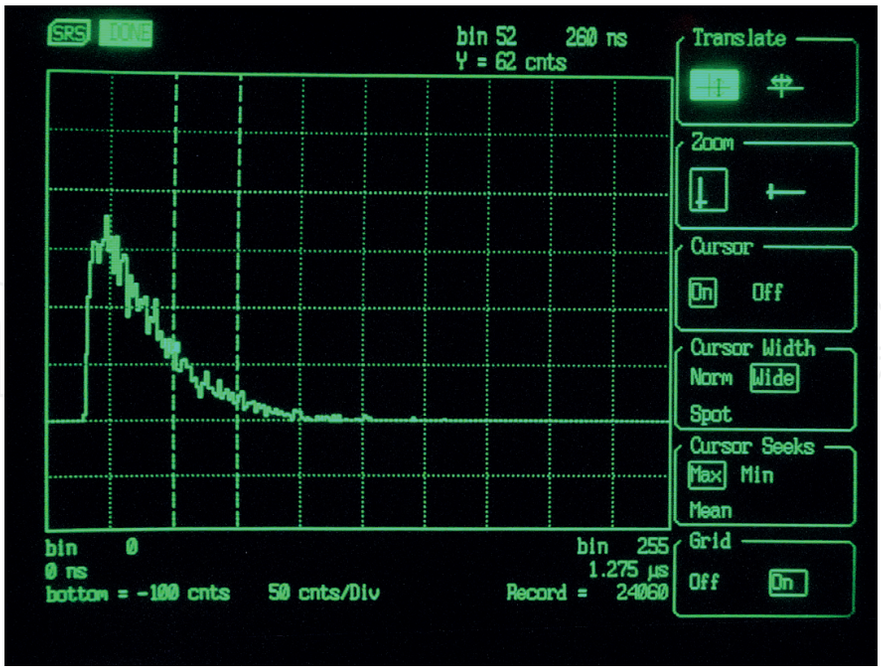

Figure 3. Photon counter system.

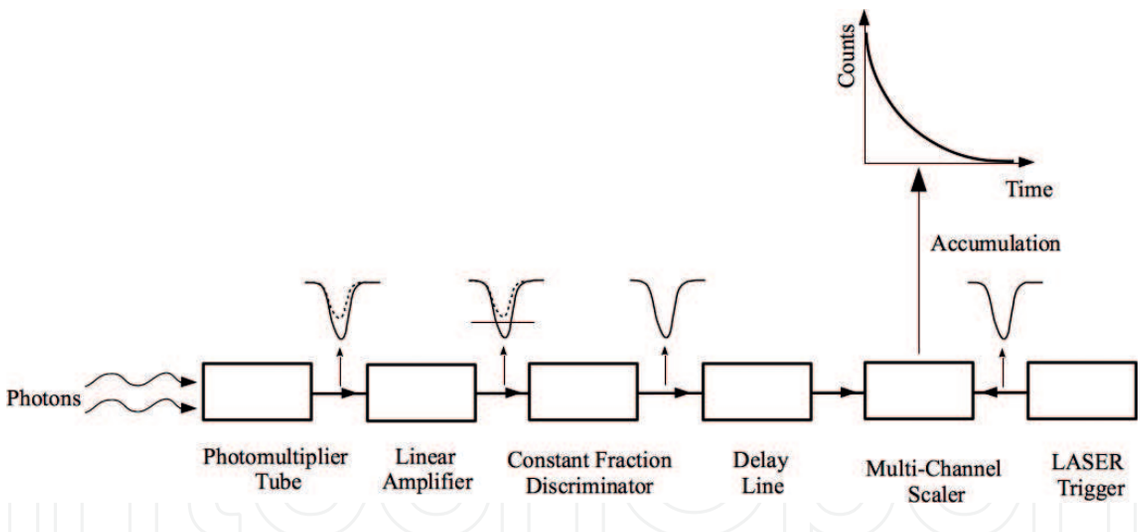

Figure 4. Laser-induced fluorescence decay recorded with a Stanford research (SR 430) multichannel Scaler (bin width, 5 ns; number of bins, 16,384; number of records, 4196).

In most cases, the luminous flux detected being rather weak, the histograms recorded are characterized by a large number of bins and a low counting rate per bin width.

The single-photon counting method is effective when the probability of detection of a single photon is greater than the probability of detection of a more than one photon. Therefore, each count corresponds to an individual incident photon, and these incident photons are detected as separate pulses. This is the case if the pulse-to-pulse interval is much greater than the pulse width.

3.3. Detection probability

Using a photomultiplier, when the average number of incident photons is $\overline{n}$, the probability of observing exactly y counts per time unit is given by the Poisson distribution:

$$P(y,\overline{n}) = \frac{(\eta\overline{n})^y}{y!} e^{-\eta\overline{n}} \tag{7}$$

where η is the quantum efficiency of the photomultiplier. η is the ratio of the average number of emitted photoelectrons from the photocathode per time unit to the average number of photon incident on the photocathode. For VUV fluorescence detection, a solar-blind photomultiplier was used with a Cs-I photocathode and MgF_2 window. The sensitivity of these photomultipliers is in the range of 110 to 200 nm, and the efficiency reaches typically 15% at maximum.

If the incident number of photons is sufficiently low, the probability of detection of photoelectrons is proportional to the number of incident photons:

$$P(y \geq 1,\overline{n}) \approx \eta\overline{n} \tag{8}$$

The detection of photoelectrons is unlikely, but when it occurs, a single photoelectron is detected because the probability of detection of more than a photoelectron vanishes.

4. Experimental methods

4.1. LIF setup

The updated experimental setup for LIF experiments shown in **Figure 5** is designed to the selective excitation by multiphotonic absorption of the first resonant or metastable states of rare gases (argon, krypton and xenon) and to the recording of the VUV fluorescence decay of rare-gas excimers or exciplexes.

The excitation wavelength range was obtained with the frequency-doubled light of a laser beam coming from a two-stage dye laser amplifier (Sirah Cobra Stretch) pumped by the second or the third harmonic beam of a neodymium YAG laser (Spectra-Physics). A spectral width of 0.002 nm was obtained with a double-grating oscillator. Typically, the dye laser operates in the visible spectral range, and the frequency of the dye laser beam is doubled by a BBO crystal followed by a compensator. The pulse duration of the frequency-doubled beam did not exceed $\tau_L = 7$ ns with a repetition rate of 30 Hz. The UV laser pulse energy is measured with an energy meter (Ophir Nova II) equipped with a pyroelectric energy sensor. The laser energy of the output beam is controlled by a motorized variable laser attenuator (Standard 10 MVAA) having an extremely low output beam deviation and a wide spectral range emission flux variation.

The vertically polarized VUV laser beam entered a cylindrical stainless steel chamber, and it provided excitation along the cell's axis. The luminescence was observed perpendicularly to the laser beam, through a magnesium fluoride porthole, by means of a VUV photomultiplier tube (PMT: EMR-510G 'extremely solar blind') working in a single-photon counting mode. The

http://dx.doi.org/10.5772/intechopen.71942

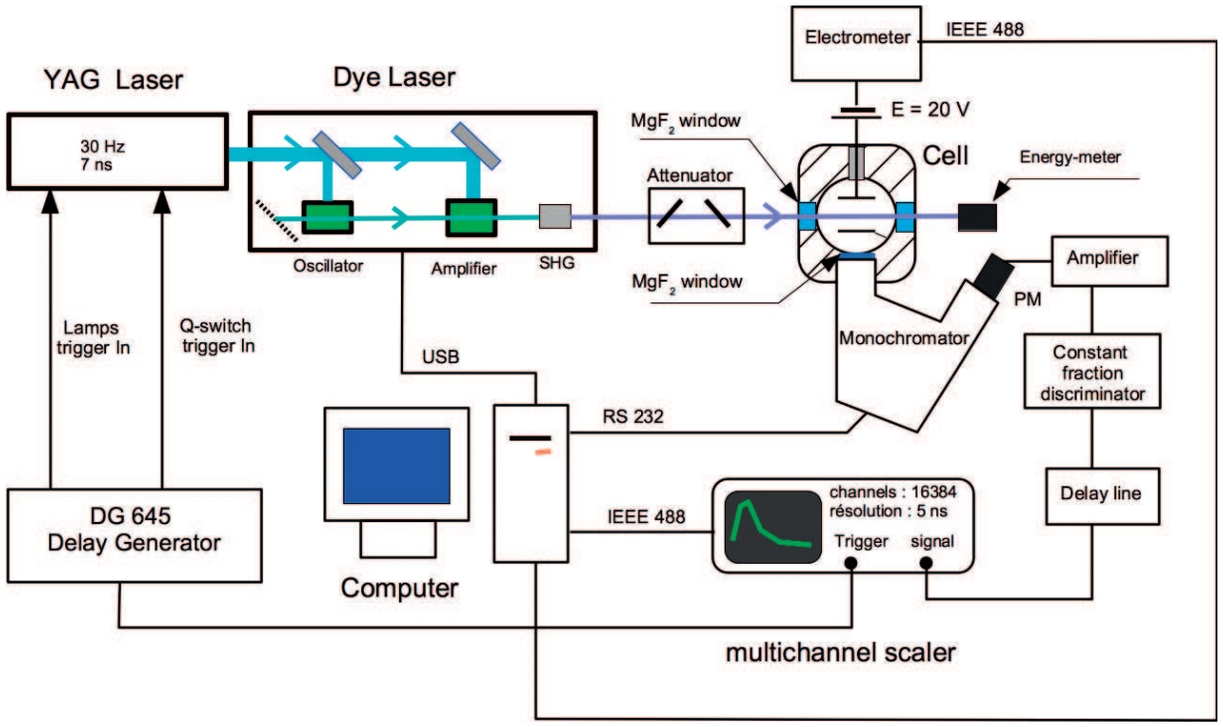

Figure 5. Schematic view of the LIF experimental setup.

detection wavelength was selected by either a VUV McPherson monochromator, for the recording of the emission spectra, or an interferential filter, for the excitation spectra and fluorescence decay recordings. The time dependence of the luminescence was monitored by using a multichannel scaler Stanford Research SR430 with 16,384 channels and a time resolution of 5 ns. The laser and the multichannel scaler were triggered by a digital delay-pulse generator (Stanford Research DG 645). An electrometer may also be added to record ionization spectra and to control multiphotonic ionization. The laser beam was on the axis of a plane capacitor where a dc electric field of 40 V cm^{-1} was applied. The charges were collected with a Keithley 617 electrometer, which could measure electric currents as low as 10 fA.

Table 1 displays some examples of configurations of the lasers used in our studies in accordance with the excited state in the case of argon, krypton and xenon (Racah notation is used).

4.2. Experimental histograms

Figure 6 shows an experimental histogram recorded at ≈128 nm representative of the fluorescence decay of the second continuum of argon following the excitation of the $Ar4s[3/2]_1$ state.

State	YAG wavelength	Dye	Output laser wavelength range	Multiphotonic process
$Ar4s[3/2]_1$	532 nm	DCM	300–330 nm	Three-photon absorption
$Kr5s[3/2]_2$	355 nm	Coumarin 307	240–270 nm	Two-photon absorption
$Xe6s[3/2]_2$	532 nm	Rhodamine B	284–307 nm	Two-photon absorption

Table 1. Laser dyes and multiphotonic process involved in kinetic studies of rare gases.

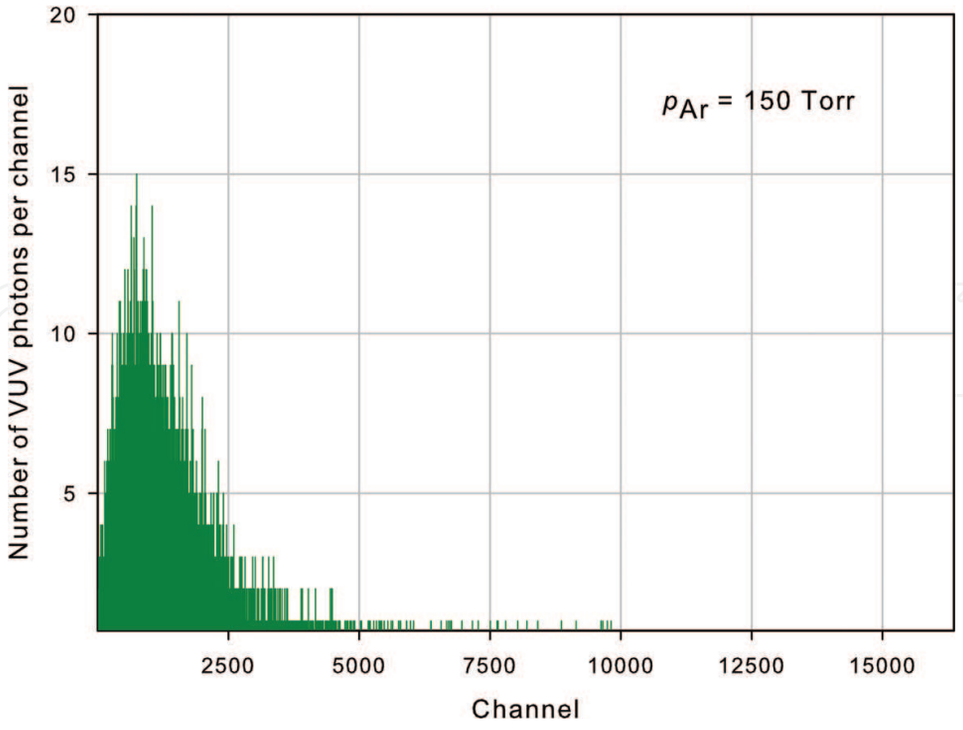

Figure 6. Experimental histogram of the VUV fluorescence following Ar4s[3/2]$_1$ selective excitation by three-photon absorption (LIF p_{Ar}, 150 Torr; λ_{em}, 128 nm; R, 5 ns) [15].

Typically, the recorded histograms are characterized by a large number of channels or bins (N_C = 16,384) and a low bin width (time resolution, R = 5 ns). For that emission wavelength, the quantum efficiency of the photomultiplier is η = 0.15. The photon counting system provides input pulses of width ≈2 ns. This histogram was recorded during 18,000 LASER pulses. This count is the accumulation number (N_A). The total VUV fluorescence acquisition time is $t_{ac} = N_C \times R \times N_A = 3.52$ s. The number of photoelectrons detected is about N_{PE} = 10,000, and the maximum of counts per channel is N_{PEmax} = 15. In average, during this experiment, the probability of counting one photoelectron during a bin width is less than 1.5×10^{-5} and reaches 3.5×10^{-4} at maximum. The pulse-to-pulse interval is more than 15 μs that is larger than the photoelectron pulse width. Thus, single-photon counting conditions are fully met.

To understand the mechanisms of formation and decay of rare-gas excimers, the histograms recorded at different pressures must be analyzed to determinate the frequency decay rates and also the lifetimes of the radiative states and the quenching rates.

5. Methods for fitting multiexponential histograms of the fluorescence decay

The luminescence decay curves follow a multiple exponential form after short laser excitation. Two methods for the curve fitting of multi-exponentials to experimental data have been compared. The chosen method needs to be accurate if the experimental signal contains exponential components with similar decay rates or both fast and slow decay rates.

5.1. Maximum likelihood method derived from a Poisson distribution

The luminescence decay curves $f(t)$ follow multiple exponential form:

$$f(t) = \sum_{p=1}^{p=D} a_p e^{-b_p t} + a_0. \tag{9}$$

The fitting method allows to obtain the amplitudes a_{p} and the decay frequencies b_{p}. The number D of exponential terms depends on the number of states involved in the process of decay. For the sake of concision and clarity, let $\theta = (a_0, a_1, \ldots, a_D, b_1, \ldots, b_D)$ be the $2D + 1$ dimension vector of unknown parameters of the function $f(t)$.

For fitting multi-exponential decay curves to experimental data, many methods of data analysis can be proposed to minimize the least squares deviation. The estimator to be minimized is

$$\Phi = \sum_{i=1}^{i=N_C} \frac{1}{\sigma_i^2} \left(y_i - f(t_i, \theta)\right)^2 \tag{10}$$

where N_{C} is the number of channels (bins) of the histogram, y_{i} is the number of counts for the i^{th} channel observed at time t_{i} and σ_{i} is the standard deviation of the statistical distribution. Here, $\sigma_i^2 = y_i$ (Poisson distribution).

Taking into account the weak probability $p(y_{\mathrm{i}})$ of detection of y_{i} counts in the *ith* channel at time t_{i} given by Poisson's law

$$P(y_i) = \frac{(f(t_i, \theta))^{y_i}}{y_i!} f(t_i, \theta) \tag{11}$$

another estimator is more relevant: the likelihood function defined as the product of the probabilities:

$$L = \prod_{i=1}^{i=N_C} \left[\frac{(f(t_i, \theta))^{y_i}}{y_i!} f(t_i, \theta)\right] \tag{12}$$

The objective of fitting method is to determine the θ parameter that maximizes the likelihood function.

Gradient vanishing $\frac{\partial L}{\partial \theta} = 0$ leads to the non-linear systems of D equations:

$$\sum_{i=1}^{i=N_C} \left(\frac{y_i}{f(t_i, \theta)} - 1\right) \frac{\partial f(t_i, \theta)}{\partial \theta} = 0 \tag{13}$$

with

$$\frac{\partial L}{\partial \theta_p} = L \left[\sum_{i=1}^{i=N_C} \left(\frac{y_i}{f(t_i, \theta)} - 1\right) \frac{\partial f(t_i, \theta)}{\partial \theta_p}\right] \quad with\ p = 1, \ldots, 2D + 1 \tag{14}$$

The function f(t) can be specified introducing the resolution R of the system of detection (e.g. the bin width of the histograms) and the channel number i:

$$f(i) = \sum_{p=1}^{p=D} a_p e^{-R(i-1)b_p} + a_0 \tag{15}$$

Thus, a new set of equations is obtained:

$$\begin{cases} \sum_{i=1}^{i=N_C} \left(\frac{y_i}{f(i)} - 1 \right) = 0 \\ \sum_{i=1}^{i=N_C} y_i \frac{e^{-R(i-1)b_p}}{f(i)} - \sum_{i=1}^{i=N_C} e^{-R(i-1)b_p} = 0 \qquad with\ p = 1, \ldots, D \\ \sum_{i=1}^{i=N_C} y_i (i-1) \frac{e^{-R(i-1)b_p}}{f(i)} - \sum_{i=1}^{i=N_C} (i-1) e^{-R(i-1)b_p} = 0 \end{cases} \tag{16}$$

These equations are solved numerically using the Newton-Raphson method. The iterative root-finding procedures of the Newton-Raphson method need an initial estimate θ_0 graphically obtained. Then, an improved estimate θ_u is produced after u iterations. The iterations go on until the relative variations of the estimate θ become negligible.

Linear equations are obtained with a first-order Taylor development of the non-linear equations about the estimate θ_u. Thus, the system of linear equations is solved with a classical Gauss algorithm.

5.2. Numerical simulations

For a simulated data derived from experimental fluorescence decays of the second continuum of krypton in krypton-xenon mixtures [17]. The exact value of the fluorescence decay is

$$f(t) = 10e^{-10^5 t} + 400e^{-2\times10^6 t} - 500e^{-1.5\times10^7 t} \tag{17}$$

Different data were simulated using a Monte Carlo method with a number of total accumulated counts varying from from 500 to 500 000. The simulated data were fluctuated by a Poisson distribution.

An example of simulated data is shown in **Figure 7**. Typically, the histograms recorded are characterized by a large number of N_C channels and a low counting rate per R = 5 ns width channel. This allows to measure with the same recording, the simultaneous measurement of both slow and fast decay rates with the same resolution and without time integration.

The decay frequency values (b_1, b_2, b_3) resulting from a least squares fit or a likelihood fit were compared to exact values. Estimation of uncertainties was performed through a statistical analysis (Type A evaluation) [25]. The standard deviation of the first convergent values was combined with the standard deviation of estimation of the decay frequencies obtained by processing the numerical method with a series of Monte Carlo-simulated histograms.

The mean values and standard deviations of the parameter estimations are summarized in **Figure 8**.

http://dx.doi.org/10.5772/intechopen.71942

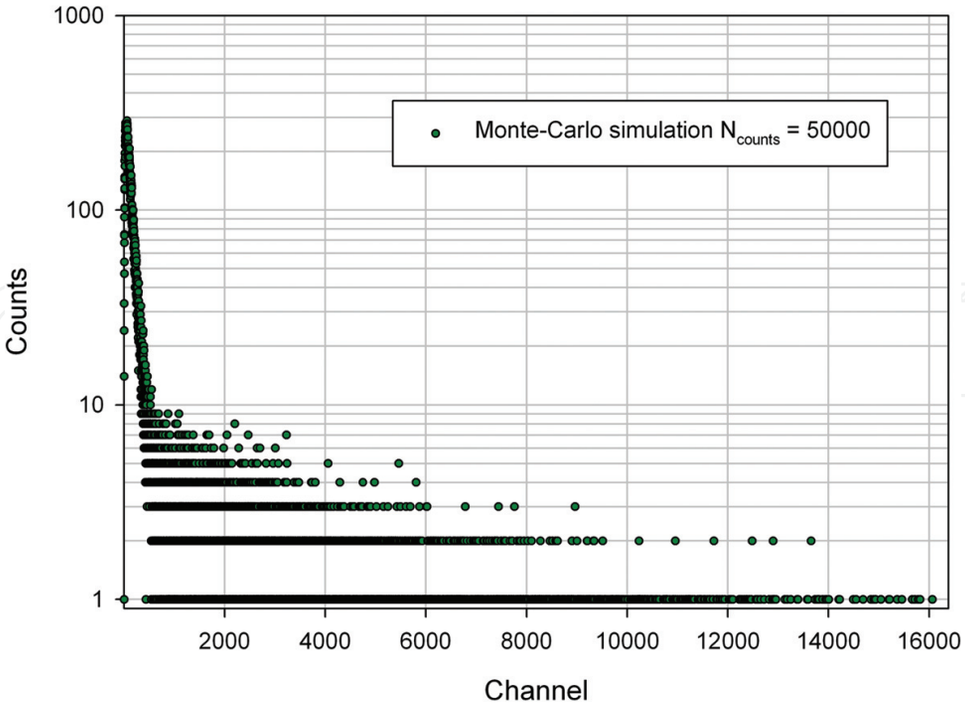

Figure 7. Simulated histogram of the VUV fluorescence (N_C, 16,384; R, 5 ns).

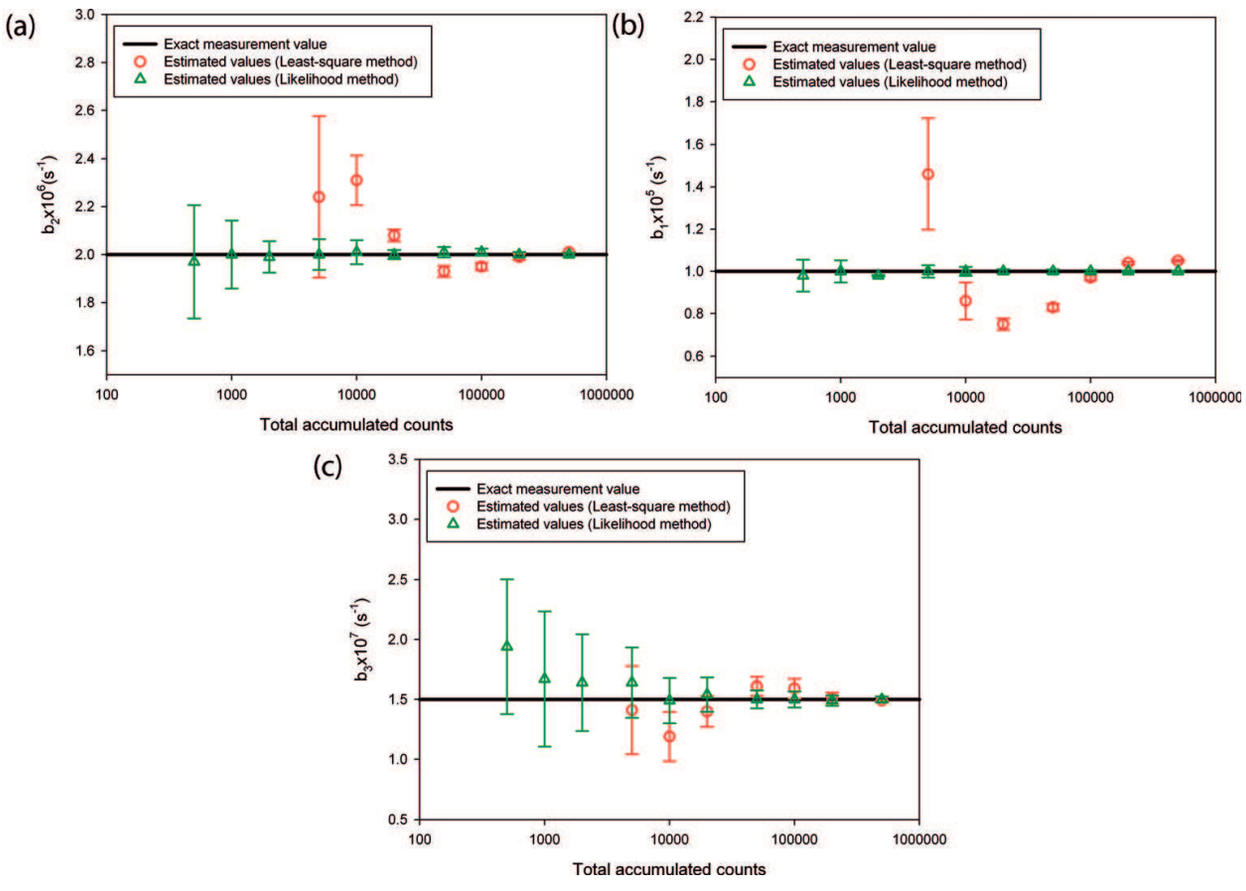

Figure 8. Estimated and exact values of the decay frequencies b_1 (figure 8-a), b_2 (figure 8-b), b_3 (figure 8-c).

Least squares method gives accurate results for high counting rates, but the method does not converge for low counting rates when the number count per channel is weak and many zeros are recorded per channel. As already demonstrated in the case of time-correlated single-photon counting (TCSPC) fluorescence decay analysis [24], the maximum likelihood method gives stable results over the whole count range, even for total counts less than 1000, where the least squares analysis delivers unreasonable values or does not converge.

For low counting rates, the maximum likelihood method gives excellent parameter estimations for multi-exponential fits of fluorescence decay curves. This method is ideally suitable for estimating the decay frequencies when the fluorescence decays are recorded with a single-photon counting system.

6. Application to the kinetic studies of rare gases

The kinetic studies following the selective excitation of the first metastable or resonant atomic states and of g or u molecular dissociative states correlated to these atomic states are highly relevant. Indeed, in operating conditions of applications, excimer production in discharges is obtained by populating relay states of higher configuration than the first metastable and resonant states, but the latter are quickly populated because the radiative and collisional decay frequencies of these higher states are fast. Finally, the $A1_u$ as well as the $B0^+_g$ molecular states are at the origin of VUV emissions. Molecular transitions can also intervene in these cascades, and the dissociative g states can serve as intermediates in populating the first metastable or resonant atomic states.

Laser-selective excitation of the first metastable state or the g parity molecular states can only be achieved with absorption of two photons, while selective excitation of the first resonant state or the u parity molecular states is done by absorption of three photons. The single-photon counting method adapted to laser-induced fluorescence kinetic studies of rare gases ensures to accurate determinations of the rate constants k_p for each decay frequency b_p involved in the VUV fluorescence decay. The values of the rate constants, k_{1p}, k_{2p} and k_{3p}, are determined using the least squares method by processing all the experimental data of the decay frequencies measured in a range of rare-gas pressures. The combined standard uncertainties of the constant rates were estimated according to the ISO Guide to the Expression of Uncertainty in Measurement [25]. Full details about the method used for the estimation of uncertainties can be found in Ref. [15].

6.1. Example of results from analyses of VUV emissions of xenon excimers in pure xenon

A comparative kinetic study of the first and second continua following the excitation of either the dissociative g molecular states correlated to $Xe6s[3/2]_1$ state or the $Xe6s[3/2]_2$ state by two-photon absorption has been performed by our team for the first time in a wide range of pressure up to 600 Torr.

Two or three frequency decay rates, depending on the initial state populated, characterize the time evolution of the second continuum of xenon. The pressure dependence (**Figure 9**) of these

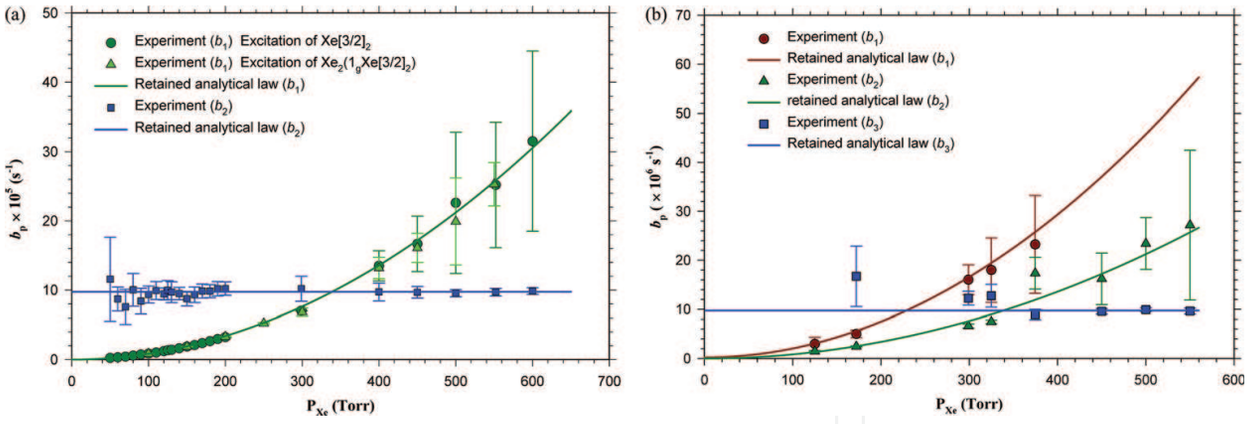

Figure 9. Decay frequencies b_1, b_2 and b_3 relative to the second continuum emission (λ_{em}, 168 nm; FWHM, 17.5 nm) versus the xenon pressure P_{Xe} following (a) an excitation of Xe[3/2]$_2$ and Xe$_2$[1 g [3/2]$_2$] and (b) excitation of Xe$_2$ [1 g [3/2]$_1$].

decay frequencies allows to determine the formation and decay mechanisms of the xenon excimers.

The first decay frequency b_1 is attributed to the decay of the metastable state by collisions with two ground-state xenon atoms:

$$\mathrm{Xe}[3/2]_2 + 2\mathrm{Xe}\left(^1S_0\right) \xrightarrow{k_{21}p_{Xe}^2} Xe_2\left(A1_u[3/2]_2\right)_{high\ v} + \mathrm{Xe}\left(^1S_0\right) \tag{18}$$

The second decay time b_2 is unambiguously identified as the lifetime of the lowest vibrational levels of the state $1_u[3/2]_2$ (or the $O_u^-[3/2]_2$ state):

$$Xe_2\left(1u[3/2]_2\right)_{low\ v} \xrightarrow{b_2} Xe_2\left(BO_g^+\left(^1S_0\right)\right) + h\nu_{2nd\ continuum} \tag{19}$$

The third decay frequency, only observed when the resonant state is initially populated, corresponds to the decay of the resonant state by collisions with two ground-state xenon atoms:

$$\mathrm{Xe}[3/2]_1 + 2\mathrm{Xe}\left(^1S_0\right) \xrightarrow{k_{31}p_{Xe}^2} Xe_2\left(BO_u^+[3/2]_1\right)_{high\ v} + \mathrm{Xe}\left(^1S_0\right) \tag{20}$$

The kinetic study of formation and decay of xenon excimer combined with the spectroscopic studies allows establishing a kinetic scheme describing all the radiative and collisional mechanisms involved in the VUV emission of xenon [16] (**Figure 10**).

Three-body rate constants relative to the formation of excimers and radiative lifetime of $Xe_2\left(A1_u[3/2]_2\right)_{lowv}$ are consistent with those reported in the literature [26–28] and are more accurate.

Analysis of the amplitudes of the fluorescence decays allowed the determination of the binary collision rate constant for vibrational relaxation and energy transfer arising from the high vibrational levels of the xenon excimer correlated to the resonant state toward the metastable.

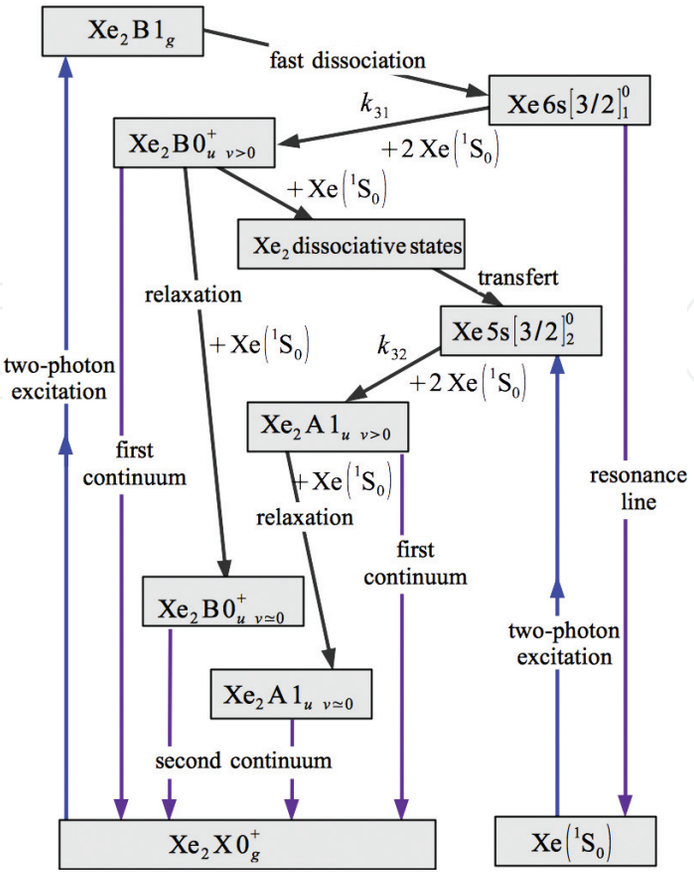

Figure 10. Kinetic scheme of formation and decay of xenon excimers when the first resonant or metastable states of xenon are initially populated.

6.2. Other rare gases and mixtures

Studies of VUV emission using two- or three-photon absorption laser-induced fluorescence (TALIF) technique were undertaken in argon and krypton. The decays of the first resonant and the first metastable state of argon $Ar4s[3/2]_1$ and $Ar4s[3/2]_2$ or $Kr5s[3/2]_1$ and $Kr5s[3/2]_2$ were explained with respect to the kinetic model already proposed for xenon [15, 20].

The decay of the first resonant state leads to very efficient population of the metastable via the molecular state $(B0_u^+)_{highv}$ and dissociative states correlated with the metastable state. Thus, at high pressure, emission of the second continuum comes from radiative de-excitation of the excimer states $(A1_u)_{lowv}$ toward the molecular ground state. The study of the temporal behavior of the second continuum of argon shows the formation of excimers only by three-body collisions. The three-body rate constant of formation was measured for the first time under selective excitation of the first resonant state of argon and the first resonant and metastable state of krypton (**Table 2**). All these studies allow the clarification of the mechanisms of VUV emission involved in the dielectric barrier discharge.

More complex kinetic schemes were proposed in Kr-Xe mixtures [17]. In mixtures, instead of the continuum of krypton, when a small amount of xenon was added, the first and second continua of xenon were observed, even though $Kr5s[3/2]_1$ was initially excited, proving the

Rare gas	k_{31} (10^{-32} cm^6 s^{-1})	k_{31} (10^{-32} cm^6 s^{-1})	τ_{1_u} (ns)
Argon		1.81 ± 0.18	3090 ± 50
Krypton	9.24 ± 0.80	3.81 ± 0.08	261.6 ± 5.7
Xenon	16.9 ± 1.4	7.87 ± 0.09	102.6 ± 1.3

Table 2. Three-body rate constants relative to the decay of the first resonant (k_{31}) and the first metastable state (k_{32}) and lifetime of the a[1u[3/2]$_1$] excimer.

efficiency of the energy transfer. From the temporal analysis in pure krypton, the three-body rate constants for Kr5s[3/2]$_1$ and Kr5s[3/2]$_2$ and the lifetime of the excimer Kr_2A1_u have been measured again. In the mixtures, we clearly showed the occurrence of an energy transfer from Kr5s[3/2]$_1$ to the Xe[5d(7/2)3] level, and the two-body collision rate constant has been estimated. A weak coupling could also intervene between these two states.

When the Xe5s[3/2]$_1$ or Xe6s[3/2]$_2$ were initially excited, the formation of the heteronuclear KrXe* exciplexes was clearly shown [18]. The decay frequency of heteronuclear excimers correlated to the xenon metastable state obeys different scaling laws depending on the xenon pressure. The roles of heteronuclear and homonuclear excimers in the formation of VUV emissions of the gas mixture are interpreted.

7. Rare-gas luminescence in dielectric barrier discharges

7.1. Monofilamentary dielectric barrier discharge

When performed in a neutral gas, kinetic analysis, following a brief and selective excitation of an identified state, is very reliable and proves to be a powerful tool. But, this analysis cannot be extrapolated with the same gas, subjected to discharge operating conditions, nor can it be considered as a mere juxtaposition of the kinetics of several distinct states. Nevertheless, if, on the one hand, the discharge excitation phase is quite short and, on the other one, time origin is perfectly defined, then an in situ kinetic analysis of the discharge can be achieved with the single-photon counting technique. A monofilamentary dielectric barrier discharge (MF-DBD) meets these requirements and can thus be a good candidate for such studies.

Figure 11 shows a schematic diagram of our experimental setup meant to produce spatially stable MF-DBDs. These micro-discharges were achieved in a glass cell, between two identical in-house-made electrodes in a classical double barrier discharge configuration. Each electrode was a 4 mm-diameter cylindrical aluminum rod covered with 0.5 mm-thick alumina, thus ensuring a monofilamentary micro-discharge (MF-DBD) [29]. The adjustable interelectrode distance d was set to 2 mm. A tuneable sinusoidal high voltage, $u$cell(t) ≈ $u$sup(t), was applied to the electrodes by means of a step-up ferrite transformer driven by a power amplifier. The current, $i$cell(t) ≈ $i$sup(t), flowing through the cell, consisted of a fast-rising pulse (pulsed current) superimposed on a displacement current, was obtained by measuring the voltage drop across a 50 Ω series-grounded resistance. Electric signals were recorded with a 10 GHz digital sampling 1 GHz oscilloscope (TDS7104). For each micro-discharge, the instant of origin

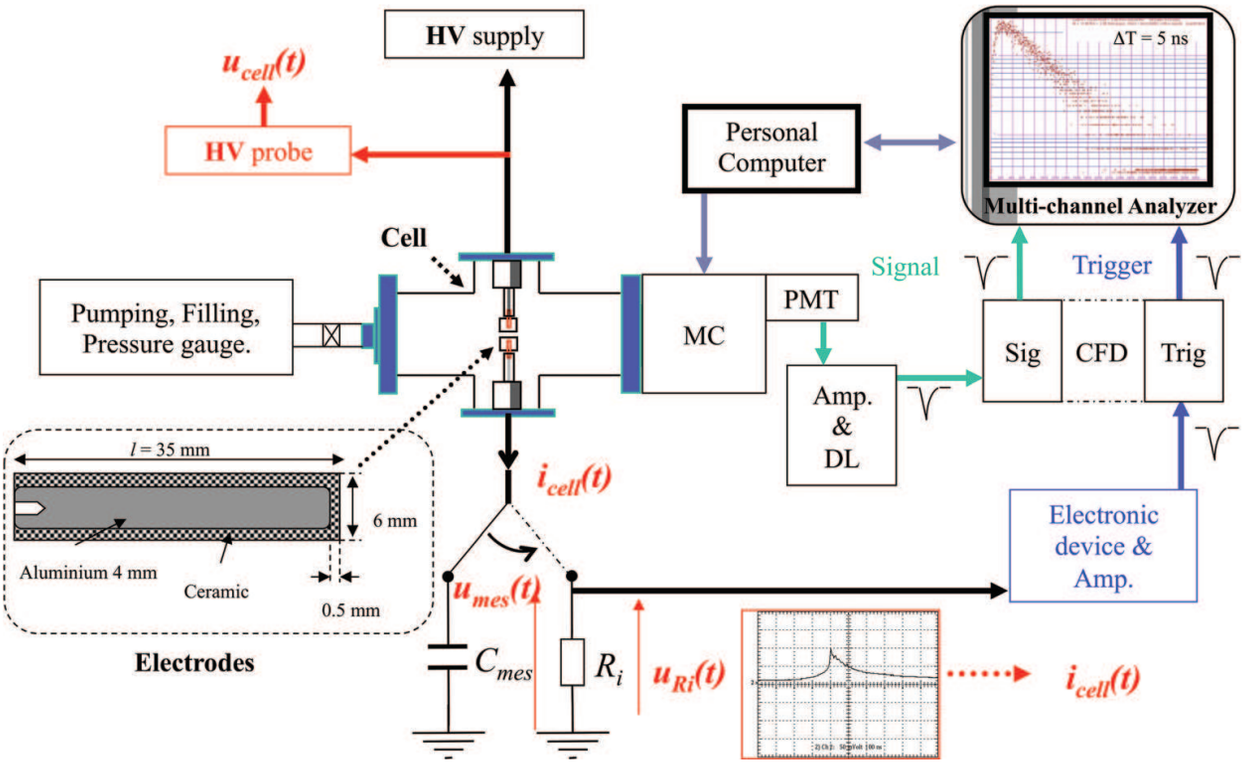

Figure 11. The experimental setup for electrical and emission spectroscopic analysis of MF-DBDs.

for photon counting was defined on the leading edge of the fast cell current pulse, using a constant fraction discriminator.

High-speed photography of the micro-discharge was performed with a 3 ns gated intensified charge-coupled device (ICCD) 512 × 512 array camera (PI-MAX Princeton Instruments) covering the visible to near-infrared spectrum (360–920 nm). Snapshots of the global visible luminescence were taken at regular intervals of 4 ns with an exposure time of 3 ns by accumulating 2000 micro-discharges on the positive half cycle. For each snapshot of the ICCD camera, triggering was performed on the leading edge of the preceding negative current pulse and with a constant delay of about half the signal period. During the high-speed photography of the discharge, the statistical fluctuations on the time lag between two successive current pulses for 2000 events corresponded to a pulse-to-pulse jitter (external jitter) of 3 ns. So, the time position of each snapshot was known with an uncertainty of about 3 ns. The cell was filled with laboratory-grade pure argon, xenon or krypton. Before filling up at the required pressure, the cell was evacuated down to at least 10^{-7} Torr. During filling up, the gas was drifted through an aluminum-zirconium getter pump for further purification.

The VUV emissions were recorded with the same device used for LIF experiments and processed with the same numerical techniques (**Figure 12**).

7.2. Electrical waveforms and discharge development

The development of a single micro-discharge is clearly shown by the successive snapshots given in **Figure 13a**, together with the cell current depicted in **Figure 13b** on an expanded time scale. The rhombuses correspond to the first six snapshots given in **Figure 13a**.

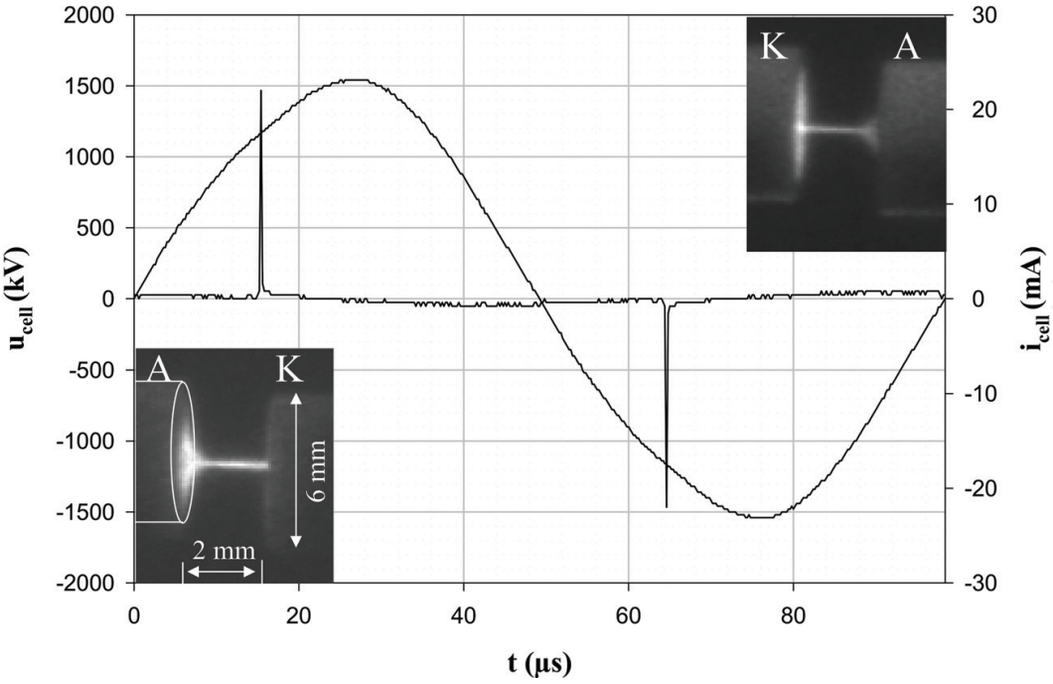

Figure 12. Supply voltage, cell current and 5 ns time-integrated snapshots of the discharge, in the visible range for P_{Xe}, 400 Torr; *f*, 10 kHz; *d*, 2 mm; and *U*max, 1.55 kV [36].

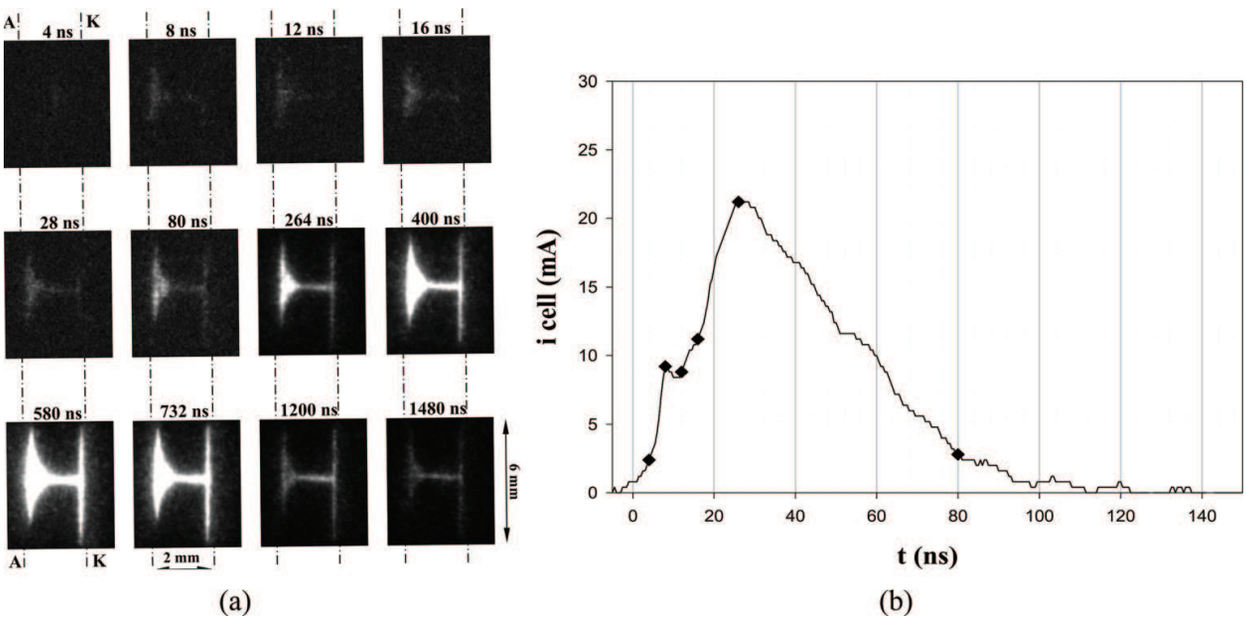

Figure 13. The micro-discharge for P_{Xe}, 200 Torr; f, 10 kHz; d, 2 mm; and Umax, 2.36 kV. (a) Evolution of the micro-discharge: 3 ns exposure time snapshots in the visible range (360 to 920 nm). The 264 ns snapshot is the reference for light intensity. A, anode; K, cathode. (b) Cell current with expanded time scale. Rhombuses correspond to the first six snapshots of (a) [36].

The cell current can be described as a main fast-rising pulse superimposed on a weak sinusoidal component. Above 200 Torr, its pulse duration is always less than 30 ns. Snapshots taken at t = 4 ns and at 8 ns show the propagation (its average speed is about 2.5×10^5 ms^{-1}) of the primary electronic avalanche reaching the anode at about t = 8 ns, for which icell shows the

characteristic peak corresponding to the arrival of this avalanche at the anode. The positive streamer (cathode-directed streamer), which is, in fact, an ionization wave due to secondary avalanches, propagates toward and reaches the cathode at about t = 16 ns, forming a conducting channel between the anode and the cathode. The diameter of the luminous filament is 0.26 mm (the maximum current density is about 320 A cm^{-2}). This value is comparable with the current density proposed by Kogelschatz [30].

Operating at 10 kHz and at low pressures, between 25 and 150 Torr (**Figure 14a**), the xenon MF-DBD emitted, within 118–300 nm, both the first and second xenon continua centered, respectively, at 152 and 172 nm, the first continua being more significant up to 150 Torr. Above 300 Torr (**Figure 14b**), only the 172 nm emission was present. No significant emission was present above 180 nm in the VUV range.

These continua of xenon were also observed in other xenon discharges [23, 31–35].

7.3. Temporal decays of the observed VUV emissions

After a time $t = t_0$, always less than 80 ns, the luminescence decays of both the first and the second continua of xenon were fairly well described, over the whole pressure domain, by a sum of exponential terms. When we included the first 80 ns in the time range of our data processing, the histograms were not correctly represented by exponential terms: the maximum likelihood computation used for the estimation of the time constants did not converge. This feature is consistent with the current flowing through the cell, showing that the currently is nearly choked after 80 ns (**Figure 15**).

For all the working xenon pressures, the luminescence decays of the first continuum were well described, after t_0, by only two exponential terms. The first decay frequency, b_1, of this emission is attributed to the decay of the $Xe[3/2]_1$ resonant state through collisions with two ground-state xenon atoms, leading to the formation of $Xe_2[B0_u^+(3/2)_1]_{highv}$ excimers with $k_{31} = (16.7 \pm 2.7)10^{-32}$ cm^6 s^{-1} and $\alpha_{11} = (1.6 \pm 0.6) \times 10^6$ s^{-1}. α_{11} is the inverse of the apparent lifetime of the $Xe[3/2]_1$ due to radiation trapping of the resonant photons in the cell. Its value depends on the cell's configuration.

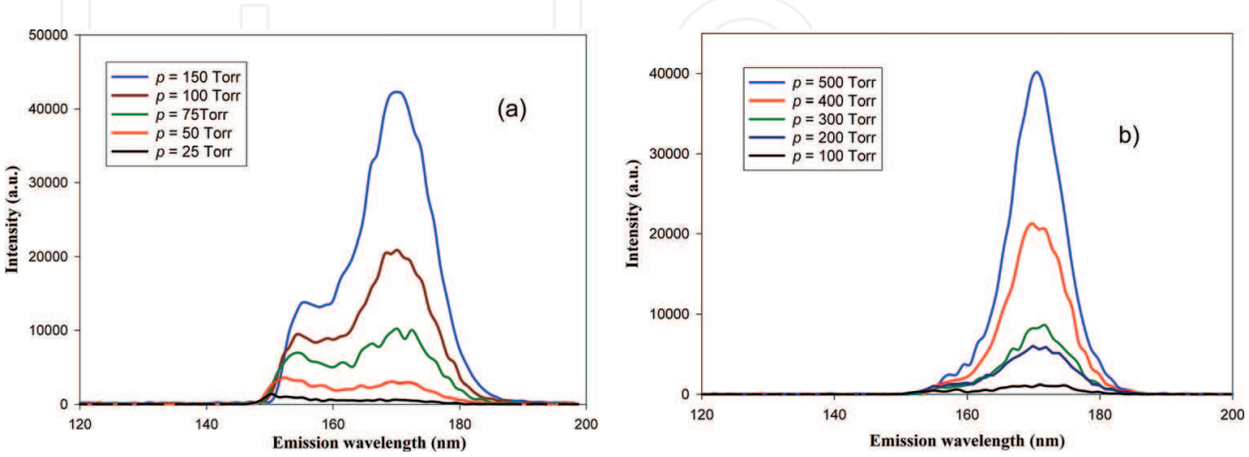

Figure 14. Emission spectra of the xenon MF-DBD at different pressures (Δλ, 1 nm): *f*, 10 kHz; *d*, 2 mm. (a) Low pressure and (b) high pressure [36].

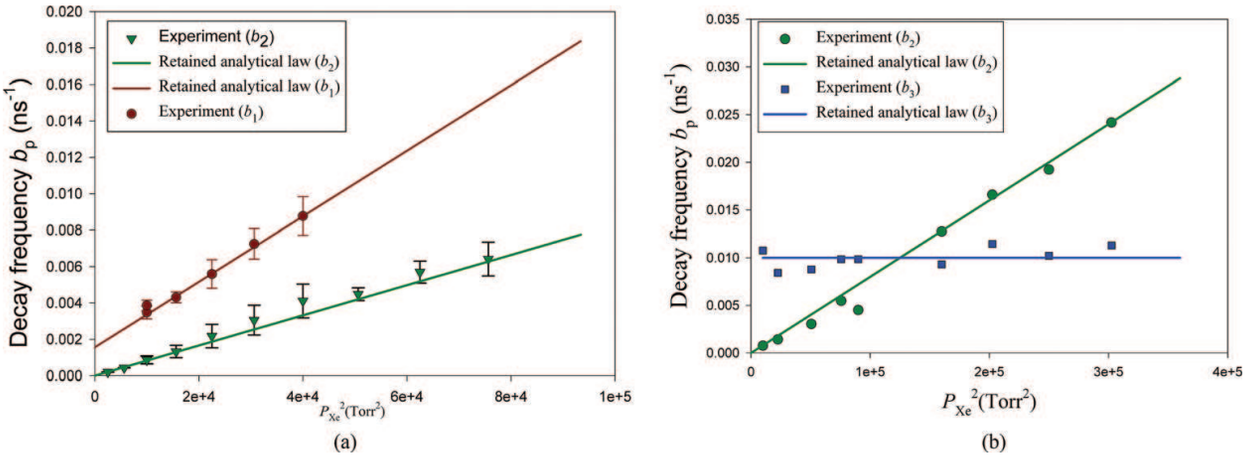

Figure 15. Decay frequencies *b*p, relative to (a) the first continuum (152 nm) and (b) the second continuum (172 nm) for *f* (10 kHz) and *d* (2 mm) versus the square of xenon pressure P_{Xe}^2 [36].

k_{31} is the three-body rate constant relative to the decay of $Xe[3/2]_1$ state, leading to the formation of $Xe_2[B0_u^+(3/2)_1]_{high\ \nu}$ excimer. Our measured value is consistent with other experimental [18, 37, 38] or theoretical works [39],where like us two-body collisions of the resonant state are not observed as well.

The second decay frequency, b_2, of the first continua is attributed to the decay of the $Xe[3/2]_2$ metastable state through collisions with two ground-state xenon atoms, leading to the formation of $Xe_2[A1_u(3/2)_2]_{high\ \nu}$ excimers [36], with $k_{32} = (7.7 \pm 1.1)\ 10^{-32}$ cm^6 s^{-1}.

After the initial active phase lasting at most 80 ns, the luminescence decays of the second continuum were fairly described, over the whole pressure domain (100 to 550 Torr), by only two exponential terms with decay frequencies b_2 and b_3. The decay frequency, b_3, of the second continua is attributed to the radiative decay of the $Xe_2[A1_u(3/2)_2]_{low\nu}$ state itself, resulting from vibrational relaxation on the $Xe_2[A1_u(3/2)_2]_{high\nu}$ excimers, through very fast binary collisions with a ground-state xenon atom. This reaction is too fast to be observed by our photon-detecting device. The radiative lifetime of the $Xe_2[A1_u(3/2)_2]_{low\nu}$ excimers is $\tau_{1u} = (96 \pm 6)$ ns. This value is concordant with literature values [16, 26, 27, 37, 38, 41, 42].

7.4. Kinetic scheme

The kinetic scheme given in **Figure 16** summarizes the main reactions occurring in the xenon MF-DBD during the post-discharge phase. Only the reactions (R-6), (R-7), (R-8) and (R-11) were directly identified in our kinetic study. Reactions (R-3), (R-4), (R-9) and (R-10) were indirectly identified but are too fast to be measured by our detecting device. Finally, reactions (R-1) and (R-2) were not observed in the kinetic study, but they were identified in our emission spectra at low pressures.

At early stages, electrons and ions, as well as higher excited states, are present in the discharge. Electrons likely excite the lowest resonant and metastable states, which are also indirectly populated via fast cascades issuing from these highly excited states. All these reactions occur

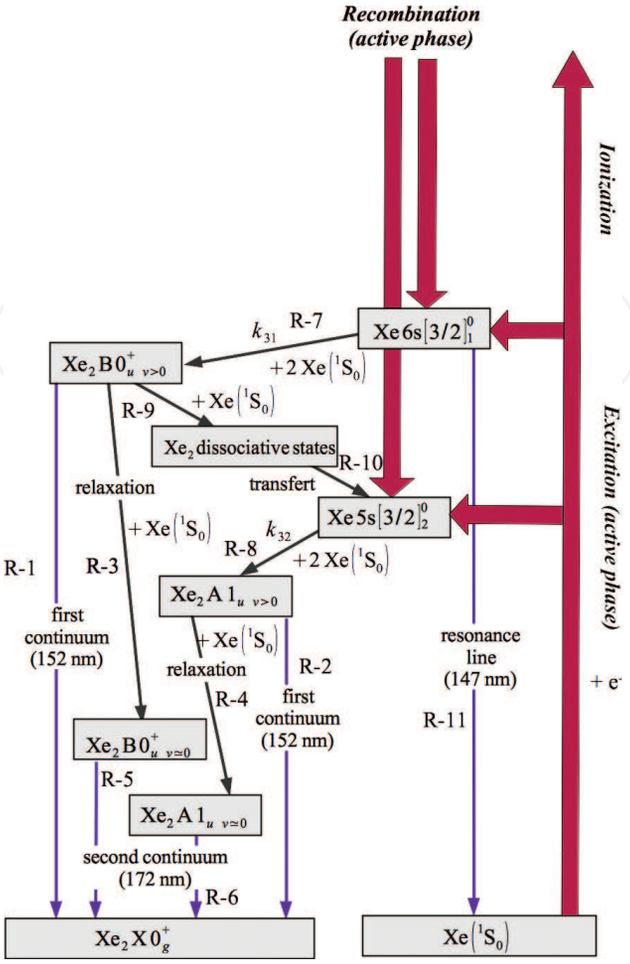

Figure 16. Kinetic scheme of the post-discharge in a high-pressure xenon MF-DBD.

during the first 80 ns, while the current is extinguished within 30 ns. Finally, these reactions lead to the formation of $Xe_2[A1_u(3/2)_2]_{high\nu}$ and then $Xe_2[A1u(3/2)_2]_{low\nu}$ which emits, nearly exclusively, the narrow energetic second continuum.

8. Radiation trapping in rare gases

Resonant states play an important role in excimer formations and are involved in emission of UV sources based on rare gases. Atoms excited in a resonant state will decay to the ground level by emission of resonant photons themselves having a good probability of being absorbed by surrounding ground-state atoms and then reemitted. Imprisonment of resonance radiation or radiative trapping is caused by multiple emission, absorption and re-emission of photons before they leave the cell [28, 40].

The escape factor g which characterizes this process is defined as the mean number of absorption-reemission processes. It depends on both the gas used and the geometrical characteristics of the experimental device. The measured apparent lifetime τ_a is expressed as a function of the natural lifetime τ_n: $\tau_a = g\,\tau_n$.

Each time a photon is reabsorbed, it can be lost by collisional quenching of the resonant atomic state. So, resonance radiation trapping allows collisional decay to prevail over radiative decay, permitting excimer formation from resonant states.

8.1. Experimental results in pure xenon

The selective excitation of $Xe[3/2]_1$ was achieved by three-photon excitation using a tunable laser. The luminescence of the first resonance line and the first continuum of xenon was observed through an interferential filter centered at 145 nm (FWMH = 17.5 nm). Luminescence was recorded by means of a VUV photomultiplier set in the photon counting mode.

When the pressure is less than 15 Torr, the temporal luminescence decay is well described by a single exponential term. The variation law of the decay frequency (b_1) is parabolic $\left(b_1 = \ \alpha_{11} + k_{31}N_{Xe}^2\right)$.

With $\alpha_{11} = 1/\tau a = 2{,}64.10^5\ s^{-1}$ and $k_{31} = (20.1 \pm 1.1)\ 10^{-32}\ cm^6\ s^{-1}$.

This time constant is attributed to the $Xe[3/2]_1$ state, and the apparent lifetime is 3.79 μs. The natural lifetime is equal to 3.98 ns [26]. The escape factor g = 952: a photon undergoes 952 absorption-re-emission processes, on average, until it leaves the cell in our experimental conditions. Constant k_{31} expresses excimer formation:

$$Xe\left(^3P_1\right) + 2Xe\left(^1S_0\right) \rightarrow \ Xe_2\ \left(O_u^+\left(^3P_1\right) high\, v\right) + Xe\left(^1S_0\right) \tag{21}$$

A second exponential term appears only for pressures greater than 15 Torr. The best fit of b_2 gives $\left(b_2 = k_{32}N_{Xe}^2\right)$.

The absence of a constant term suggests an excited state with a long lifetime. This time constant was attributed to the $Xe[3/2]_2$ metastable state. This state is created during the vibrational relaxation of the O_u^+ state.

8.2. Experimental results in xenon-krypton mixtures

This study was performed in the same excitation and detection conditions as for pure xenon. This study shows that the foreign gas (krypton) at high concentration modifies trapping phenomena and that van der Waals broadening by krypton should be taken into account. There exists no energy transfer between the two rare gases when the foreign gas (krypton) is lighter than the excited one (xenon).

On the contrary, efficient energy transfers occur from a lighter rare gas toward a heavier one, like in Kr-Xe mixtures following excitation of Kr.

9. Conclusion

Kinetic studies of rare-gas VUV fluorescence decays under short and selective multiphotonic excitation conditions using single-photon counting fluorescence are highly suitable for the determination of reliable kinetic models. The use of the maximum likelihood method offers

the possibility to lower excitation energies and to determinate fast and slow decay frequencies in a same scan. This allows us to determine the main mechanisms involved in the formation and decay of rare-gas excimers.

For high pressures, emission of the second continuum comes from radiative de-excitation of the excimer states correlated to the first metastable state toward the molecular ground state. The study of the temporal behavior of the second continuum of pure rare gas shows the formation of excimers only by three-body collisions. The three-body rate constant of formation of excimers was measured for the first time under selective excitation. These studies allowed us to clarify the mechanisms of VUV emission involved in the dielectric barrier discharge. Resonant states do not seem to contribute to the production of excimers in a dielectric barrier microdischarge. The resonant state contributes to the formation of excimer through the transfer toward the metastable state at high pressures. The second continuum essentially comes from radiative transition of the low vibrational levels of the excimer correlated with the metastable state.

Author details

Frédéric Marchal*, Neermalsing Sewraj, Jean-Pierre Gardou, Nofel Merbahi and Mohammed Yousfi

*Address all correspondence to: frederic.marchal@laplace.univ-tlse.fr

LAPLACE, Université de Toulouse, CNRS, INPT, UPS, France

References

[1] ChanMay BP. Biomedical applications of photochemistry. Tissue Engineering Part B: Reviews. 2010;**16**(5):509-522. DOI: https://doi.org/10.1089/ten.teb.2009.0797

[2] Truica-Marasescu F, Guimond S, Wertheimer MR. VUV-induced nitriding of polymer surfaces: Comparison with plasma treatments in nitrogen. Nuclear Instruments and Methods in Physics Research Section B: Beam Interactions with Materials and Atoms. 2003;**208**:294-299. DOI: https://doi.org/10.1016/S0168-583X(03)00658-X

[3] Halfmann H, Denis B, Bibinov N, Wunderlich J, Awakowicz P. Identification of the most efficient VUV/UV radiation for plasma based inactivation of bacillus atrophaeus spores. Journal of Physics D: Applied Physics. 2007;**40**(19):5907. DOI: https://doi.org/10.1088/0022-3727/40/19/019

[4] Kristin Zoschke, Hilmar Börnick, Eckhard Worch. Vacuum-UV radiation at 185 nm in water treatment – A review. Water Research 2014;**52**:131-145. DOI: http://dx.doi.org/10.1016/j.watres.2013.12.034

[5] Eliasson B, Kogelschatz U. UV excimer radiation from dielectric-barrier discharges. Applied Physics B. 1988;**46**(4):299-303. DOI: https://doi.org/10.1007/BF00686452

[6] Kogelschatz U. Ultraviolet excimer radiation from nonequilibrium gas discharges and its application in photophysics, photochemistry and photobiology. Journal of Optical Technology. 2012;**79**(8):484-493. DOI: https://doi.org/10.1364/JOT.79.000484

[7] Oppenländer T. Mercury-free sources of VUV/UV radiation: Application of modern excimer lamps (excilamps) for water and air treatment. Journal of Environmental Engineering and Science. 2007;**6**:253-264. DOI: https://doi.org/10.1139/s06-059

[8] Wilkinson PG, Byram ET. Rare gas light sources for the vacuum ultraviolet. Applied Optics. 1965;**4**(5):581-588. DOI: https://doi.org/10.1364/AO.4.000581

[9] Jun-Ying Zhang, Ian W. Boyd. Efficient excimer ultraviolet sources from a dielectric barrier discharge in rare-gas/halogen mixtures. Journal of Applied Physics. 1996;**80**:633. DOI: http://dx.doi.org/10.1063/1.362871

[10] Xueji Xu. Dielectric barrier discharge - properties and applications. In Thin Solid Films. 2001;**390**(1-2):237-242. https://doi.org/10.1016/S0040-6090(01)00956-7

[11] Mildren RP, Carman RJ. Enhanced performance of a dielectric barrier discharge lamp using short-pulsed excitation. Journal of Physics D: Applied Physics. 2001;**34**(1):L1. DOI: https://doi.org/10.1088/0022-3727/34/1/101

[12] Wilkinson PG, Tanaka Y. New xenon-light source for the vacuum ultraviolet. Journal of the Optical Society of America. 1955;**45**(5):344-349. DOI: https://doi.org/10.1364/JOSA.45.000344

[13] Tanaka Y. Continuous emission spectra of rare gases in the vacuum ultraviolet region. Journal of the Optical Society of America. 1955;**45**(9):710-713. DOI: https://doi.org/10.1364/JOSA.45.000710

[14] Hoff PW, Rhodes CK. Introduction. In: Rhodes Charles K, editor. Excimer Lasers. Berlin Heidelberg, New York: Springer-Verlag; 1979. pp. 1-4. DOI: https://doi.org/10.1007/978-3-662-11716-3_1

[15] Marchal F, Merbahi N, Ledru G, Gardou JP, Sewraj N. The study of VUV emissions of Ar*2 excimers using three-photon absorption laser-induced fluorescence. Journal of Physics B: Atomic, Molecular and Optical Physics. 2008;**42**(1):015201. DOI: https://doi.org/10.1088/0953-4075/42/1/015201

[16] Ledru G, Marchal F, Sewraj N, Salamero Y, Millet P. Comparative study of the formation and decay of xenon excimers following selective excitation of the 5p56s states: Spectroscopic and kinetic analysis. Journal of Physics B: Atomic, Molecular and Optical Physics. 2006;**39**(8):2031. DOI: https://doi.org/10.1088/0953-4075/39/8/020

[17] Marchal F, Berejny P, Sewraj N, Salamero Y, Millet P. Energy transfers in Kr–Xe mixtures following selective multiphotonic excitation of Kr(3P1). Temporal analysis in Kr–Xe mixtures. Journal of Physics B: Atomic, Molecular and Optical Physics. 2004;**37**(6):1279. DOI: https://doi.org/10.1088/0953-4075/37/6/012

[18] Ledru G, Marchal F, Merbahi N, Gardou JP, Sewraj N. Study of the formation and decay of KrXe* excimers at room temperature following selective excitation of the xenon 6s

states. Journal of Physics B: Atomic, Molecular and Optical Physics. 2007;**40**(10):1651. DOI: https://doi.org/10.1088/0953-4075/40/10/002

[19] Marchal F, Sewraj N, Jabbour G, Rodriguez Akerreta P, Ledru G. Temperature dependence of xenon excimer formations using two-photon absorption laser-induced fluorescence. Journal of Physics B: Atomic, Molecular and Optical Physics. 2010;**43**(23):235210. DOI: https://doi.org/10.1088/0953-4075/43/23/235210

[20] Marchal F, Jabbour G, Yousfi M, Ledru G, Sewraj N, Rodriguez-Akerreta P. Study of VUV emission of krypton using two-photon absorption laser. In: Proceedings of the 29th International Conference on Phenomena in Ionized Gases (ICPIG); 12–17 July; Cancún, Mexico. 2009. p. A-1

[21] Moutard P, Laporte P, Subtil JL, Damany N, Damany H. Pressure effects on kinetics and decay processes in argon under selective photoexcitation. The Journal of Chemical Physics. 1987;**87**:4576. DOI: http://dx.doi.org/10.1063/1.452869

[22] Hamamatsu. https://www.hamamatsu.com/us/en/technology/innovation/photoncounting/index.html [Internet]. Photon counting. Available from: https://www.hamamatsu.com/us/en/technology/innovation/photoncounting/index.html [Accessed: 05–09-2017]

[23] Mildren RP, Carman RJ. Enhanced performance of a dielectric barrier discharge lamp using short-pulsed excitation. Journal of Physics D: Applied Physics. 2001;**34**(1):L1. DOI: https://doi.org/10.1088/0022-3727/34/1/101

[24] Michael Maus, Mircea Cotlet, Johan Hofkens, Thomas Gensch and Frans C. De Schryver. An experimental comparison of the maximum likelihood estimation and nonlinear least-squares fluorescence lifetime analysis of single molecules. Analytical Chemistry. 2001;**73**(9): 2078-2086. DOI: http://dx.doi.org/10.1021/ac000877g

[25] ISO/IEC Guide98:1995, editor. Guide to the Expression of Uncertainty in Measurement (GUM). Geneva, Switzerland: ISO; 1998

[26] Bonifield TD, Rambow FHK, Walters GK, McCusker MV, Lorents DC, Gutcheck RA. Time resolved spectroscopy of xenon excimers excited by synchrotron radiation. The Journal of Chemical Physics. 1980;**72**(5):2914-2924. DOI: http://dx.doi.org/10.1063/1.439490

[27] Wenck HD, Hasnain SS, Nikitin MM, Sommer K, Zimmerer G, Haaks D. Time and spectrally resolved fluorescence of Xe molecules excited with synchrotron radiation. Chemical Physics Letters. 1979;**66**(1):138-143. DOI: http://dx.doi.org/10.1016/0009-2614(79)80384-X

[28] Sewraj N, Gardou JP, Salamero Y, Millet P. Radiation trapping of the 3P1-1S0 resonant transitions of xenon and krypton in Xe-Kr, Xe-Ar, and Kr-Ar mixtures: Kinetic analysis and determination of the van der Waals broadening coefficients. Physical Review A. 2000;**62**(5):052721. DOI: https://doi.org/10.1103/PhysRevA.62.052721

[29] Merbahi N, Sewraj N, Marchal F, Salamero Y, Millet P. Luminescence of argon in a spatially stabilized mono-filamentary dielectric barrier micro-discharge: Spectroscopic and kinetic analysis. Journal of Physics D: Applied Physics. 2004;**37**(12):1664. DOI: https://doi.org/10.1088/0022-3727/37/12/011

[30] Kogelschatz U. 10th International Conference on Gas Discharge and Applications; 13–18 September ; Swansea. 1992. p. Vol. 972–980

[31] Stockwald K, Neiger M. Some properties of a novel far UV xenon excimer barrier discharge light source. Contributions to Plasma Physics. 1995;**35**(1):15-22. DOI: http://dx.doi.org/10.1002/ctpp.2150350103

[32] Adler F, Müller S. Formation and decay mechanisms of excimer molecules in dielectric barrier discharges. Journal of Physics D: Applied Physics. 2000;**35**(14):1705. DOI: https://doi.org/10.1088/0022-3727/33/14/310

[33] Gellert B, Kogelschatz U. Generation of excimer emission in dielectric barrier discharges. Applied Physics B: Lasers and Optics. 1991;**52**(1):14-21. DOI: https://doi.org/10.1007/BF00405680

[34] Kessler F, Bauer GH. VUV excimer light source for deposition of amorphous semiconductors. Applied Surface Science. 1992;**54**:430-434. DOI: http://dx.doi.org/10.1016/0169-4332(92)90082-9

[35] Wieme W, Lenaerts J. Excimer formation in argon, krypton, and xenon discharge afterglows between 200 and 400 K . The Journal of Chemical Physics. 1981;**74**(1):483-493. DOI: http://dx.doi.org/10.1063/1.440855

[36] Sewraj N, Merbahi N, Marchal F, Ledru G, Gardou JP. VUV spectroscopy and post-discharge kinetic analysis of a pure xenon mono-filamentary dielectric barrier discharge (MF-DBD). Journal of Physics D: Applied Physics. 2009;**42**(4):045206. DOI: https://doi.org/10.1088/0022-3727/42/4/045206

[37] Salamero Y, Birot A, Brunet H, Galy J, Millet P. Kinetic study of the VUV xenon emissions using selective multiphoton excitation. The Journal of Chemical Physics. 1984;**80**(10):4774-4780. DOI: http://dx.doi.org/10.1063/1.446550

[38] Dutuit O, Gutcheck R, Calvé JL. Spectral and kinetic studies of the second continuum fluorescence of xenon excited by synchrotron radiation. Chemical Physics Letters. 1978;**58**(1):66-72. DOI: http://dx.doi.org/10.1016/0009-2614(78)80318-2

[39] Janssens H, Vanmarcke M, Desoppere E, Lenaerts J, Bouciqué R, Wieme W. A general consistent model for formation and decay of rare gas excimers in the 10^{-2}–10^{+5} mbar pressure range, with application to krypton. The Journal of Chemical Physics. 1987;**86**(9):4925-4934. https://doi.org/10.1063/1.452662

[40] Molisch AF, Oehry BP, editors. Radiation Trapping in Atomic Vapours. Oxford University Press; 1998. 536 p

[41] Keto JW, Gleason RE, Bonifield TD, Walters GK, Soley FK. Collisional mixing of the lowest bound molecular states in xenon and argon., Chemical Physics Letters. 1976;**42**(1): 125-128. DOI:, http://dx.doi.org/10.1016/0009-2614(76)80566-0

[42] Barbet A, Sadeghi N, Pebay-Peyroula JC. Decay of metastable xenon atoms Xe*(3 P 2) in a xenon afterglow. Journal of Physics B: Atomic and Molecular Physics. 1975;**8**(10):1776. DOI: https://doi.org/10.1088/0022-3700/8/10/027

IntechOpen